ACS Photonics

Article

Cite This: ACS Photonics 2019, 6, 2238−2244

pubs.acs.org/journal/apchd5

Optoelectronic Devices on Index-near-Zero Substrates

Lisa J. Krayer,[†,‡] Jongbum Kim,[‡] Joseph L. Garrett,[‡] and Jeremy N. Munday*[,†,‡]

[†]Electrical and Computer Engineering Department and [‡]Institute for Research in Electronics and Applied Physics, University of Maryland, College Park, Maryland 20742, United States

Supporting Information

ABSTRACT: Light absorption in metal films can excite hot carriers, which are useful for photodetection, solar energy conversion, and many other applications. However, metals are highly reflective, and therefore, careful optical design is required to achieve high absorption in these films. Here we utilize a subwavelength Fabry-Pérot-like resonance in conjunction with an index-near-zero (INZ) substrate to achieve near-unity absorption and hot carrier photocurrent in nanoscale metal films. By employing aluminum-doped zinc oxide (AZO) as the INZ medium in the near-infrared range, we enhance the metal film absorption by nearly a factor of 2. To exploit this absorption enhancement in an optoelectronic device, we fabricate a Schottky photodiode and find that the photocurrent generated in Pt on Si is enhanced by >80% with the INZ substrate. The enhancement arises from a combination of improved carrier generation and carrier transport resulting from the addition of the AZO film.

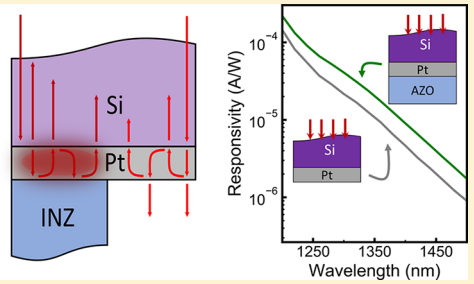

KEYWORDS: *index-near-zero materials, hot carriers, thin film absorption, photocurrent*

Interest in materials with refractive index-near-zero (INZ) has exploded in the past few years as researchers have discovered novel applications for the semi-infinite wavelengths and phase velocities of electromagnetic waves within the materials. INZ materials allow electromagnetic waves to "squeeze" through narrow channels of arbitrary geometry,[1,2] funnel light through subwavelength apertures,[3,4] further metamaterial design parameters for cloaking technology,[5] enhance optical nonlinear effects,[1,6−8] "pin" plasmonic resonances to a desired bandwidth,[9] and enable coherent perfect absorption at nanoscale film thicknesses.[10] In particular, the unique optical properties of INZ materials may be useful for optoelectronic devices by increasing the absorption in quantum-well detectors,[11] enhancing local electric fields for greater free carrier absorption for electro-optical modulation,[12,13] and coupling to metamaterial resonators for electrically tunable optical sensing.[14] While various optical effects of INZ materials have been explored, few optoelectronic devices have been fabricated to determine the combined optical and electrical impacts of INZ materials in the device design. Here we experimentally demonstrate that INZ materials can enhance both optical and electrical performance in a hot carrier photodetector.

We design a silicon-based, near-infrared (NIR) photodetector in which the photocurrent is generated within a thin metal film because of a Fabry-Pérot (FP)-like absorption resonance,[15,16] and we experimentally verify the absorption and photoresponse enhancement from an INZ substrate. To achieve INZ properties, a material must simultaneously be conductive and have low optical loss (i.e., low imaginary part of the permittivity).[17,18] INZ properties have been achieved in conductive materials where the real part of the permittivity transitions from positive to negative with low Drude damping. Feasible INZ materials include transparent conducting oxides whose carrier concentrations are suitable to achieve INZ behavior in near-infrared (NIR) wavelengths by adjusting the metal doping concentration during deposition.[6,9,19,20] For our device, we use Al:ZnO (AZO) as a low-loss INZ substrate.

A near-ideal INZ substrate with no loss (i.e. n_{inz} = 0.01) allows for near-perfect absorption in FP-like resonant thin metal films, such as Pt.[17,21] Further, we find that low levels of optical loss in the INZ substrate do not significantly impact the maximum obtainable absorption allowing for high absorption using realistic materials. In this manuscript, we experimentally determine both the absorption enhancement in ultrathin Pt films and the photoresponse enhancement in a Si/Pt Schottky photodiode resulting from the INZ properties of the AZO substrate.

RESULTS

Absorption in Metal Films Using Ideal and Nonideal INZ Substrates. Recently, it was found that a FP-like cavity can be made from planar absorbing films 10−100× thinner than the wavelength of incident light.[15,22,23] The optical loss in the films gives rise to nontrivial interference allowing for broadband absorption determined by the optical properties of the surrounding media. This concept was applied to obtain high absorption in nanometer scale semiconductor films on metallic substrates[24−26] and has also been adapted to metallic films on semiconducting substrates and exploited for hot

Received: March 23, 2019
Published: July 15, 2019

DOI: 10.1021/acsphotonics.9b00449
ACS Photonics 2019, 6, 2238−2244

carrier based photodetection.[15,21,22,27] Provided that the real (n) and imaginary (κ) parts of a metal's refractive index are approximately equal (i.e., $n \sim \kappa$) and the optical path length within the thin film is significantly shorter than the optical wavelength in free space (i.e., $2\pi d/\lambda_0 \ll 1$, where d is the film thickness and λ_0 is the wavelength in free space), the absorption within a nanoscale metal film is determined by the optical properties of the surrounding materials:[22,28]

$$A_{max} \sim \frac{n_{top}}{n_{top} + n_{bot}} \quad (1)$$

where n_{top} and n_{bot} are the real part of the refractive indices of the top and bottom layers, respectively.

According to eq 1, there are two methods of maximizing the absorption in a nanoscale metal film. The first is to ensure that $n_{top} \gg n_{bot}$. For example, when resonant films are illuminated with sub-bandgap light through silicon (i.e. $n_{top} = n_{si}$ and $n_{bot} = n_{air} = 1$), which has a refractive index of ~3.5 in the near-infrared (NIR), it is possible to obtain ~78% absorption in 15−30 nm films. The second method of maximizing absorption in a resonant film is to decrease the refractive index of the bottom material, such that n_{bot} approaches 0. In this case, A_{max} will approach 1 for any n_{top}. Here, we demonstrate this second method of maximizing absorption in a thin metal film with two examples of n_{top}: (i) $n_{top} = n_{air}$ and (ii) $n_{top} = n_{Si}$.

Figure 1 shows the FP-like absorption mechanism for both a traditional substrate ($n_{top} = n_{air}$) and one whose index approaches zero. The incident light undergoes multiple reflections within the thin film while being critically dampened, thus, requiring the film to be ultrathin. Upon partial reflection at each interface, the phase shifts accumulate to interfere with the initially reflected and transmitted waves, effectively reducing the overall reflectivity and transmittivity (Figure 1a). When an INZ substrate is used, the impedance mismatch at the metal/INZ interface increases. The high impedance mismatch both prevents any light from being transmitted into the INZ substrate and alters the phase accumulation of the partially reflected waves resulting in an increase of absorption within the metal film (Figure 1b). This absorption mechanism is the same for the case where $n_{top} = n_{Si}$; however, the initial reflection from the metal is reduced because of the lower impedance mismatch between silicon and the metal. Therefore, there is higher absorption for $n_{top} = n_{Si}$, even without the INZ substrate.

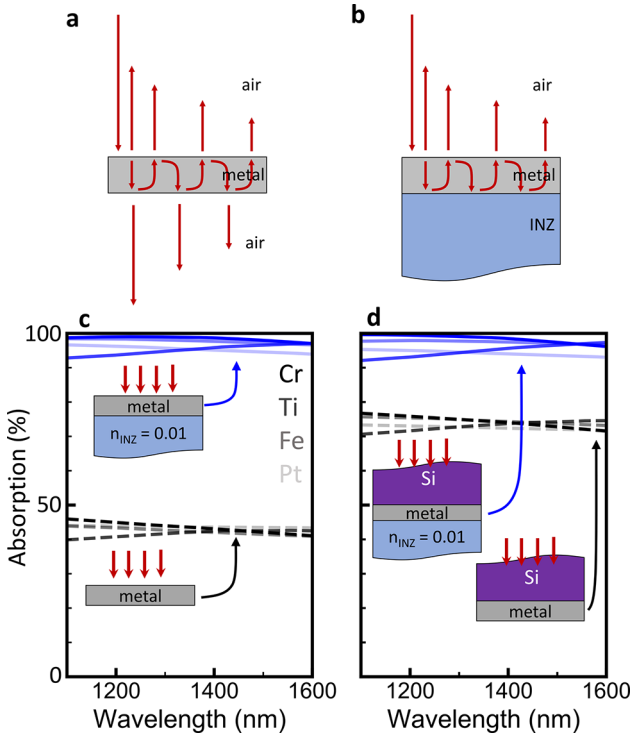

Figure 1. Near-perfect absorption in real metals on nearly ideal INZ substrates. (a) Absorption mechanism in a thin metal film suspended in air and (b) on an INZ substrate. The calculated absorption in thin film Cr, Ti, Fe and Pt illuminated from (c) air or (d) Si is near unity with an INZ substrate (n = 0.01). Solid and dashed lines are the absorption with and without the INZ substrate, respectively. The gradient in color depicts the different metals. The red arrows in the diagrams show illumination direction.

Pt, Cr, Ti, and Fe all satisfy the resonance conditions of eq 1 for high absorption,[28] and thus, they are all good candidates for near-perfect absorption with an INZ substrate. Figure 1c,d shows that the calculated absorption in these thin, resonant metals can be enhanced to near-perfect absorption with a good, no-loss INZ substrate (n = 0.01 + 0i). All absorption calculations in this manuscript were performed using the transfer matrix method,[29] and the optical properties of the metals are obtained from refs 30−32 (see Supporting Information for a description of the transfer matrix method). With light incident from free-space ($n_{top} = n_{air}$) and when an INZ substrate is used, the optimized metal film thicknesses for maximum absorption in Pt, Cr, Ti, and Fe are 3, 5, 6, and 6 nm, respectively. The INZ substrate enhances the absorption in the metal films by over a factor of 2 (Figure 1c). When light is incident from a higher index substrate ($n_{top} = n_{Si}$) rather than air, the ideal metal film thicknesses are slightly increased to 11, 16, 22, and 19 nm, respectively, and the absorption enhancement is ~30% with the addition of the INZ substrate.

Even though we approach 100% absorption in metal thin films with a nearly ideal INZ substrate, there are few known low-loss materials that have a refractive index < 0.1. In addition, such low refractive index requires the presence of optical loss from free carrier dampening and, due to dispersion, there will only be a small spectral region where both the optical loss and the real part of the refractive index are relatively low. Therefore, for realistic device considerations, it is necessary to explore the absorption enhancement from physically relevant optical properties of more realistic INZ materials.

Figure 2 shows that the presence of optical loss in the INZ substrate does not significantly change the maximum absorption, but it does impact the thin film material properties that satisfy the resonance condition. The contour plots show the numerically calculated absorption versus real and imaginary refractive indices of a 5 nm film on various INZ substrates (ranging from $\tilde{n}_{INZ}$ = 0.01 + 0.01i to $\tilde{n}_{INZ}$ = 0.75 + 0.75i), assuming illumination (λ = 1300 nm) through air (i.e., $n_{top} = n_{air}$). Both the thin film and INZ substrates have complex refractive indices labeled as $\tilde{n}_f = n_f + i\kappa_f$ and $\tilde{n}_{INZ} = n_{INZ} + i\kappa_{INZ}$, respectively.

For low n_{INZ} and κ_{INZ}, metals such as Cr, Fe, Ti, Pt, and V all lie within the absorption resonance. However, as κ_{INZ} increases (i.e., the INZ material becomes lossy) the absorption resonances move to larger n_f, shifting away from the metals listed. Interestingly, the value of the maximum absorption is independent of κ_{INZ}; instead, it is mainly dependent on n_{INZ}.

DOI: 10.1021/acsphotonics.9b00449
ACS Photonics 2019, 6, 2238−2244

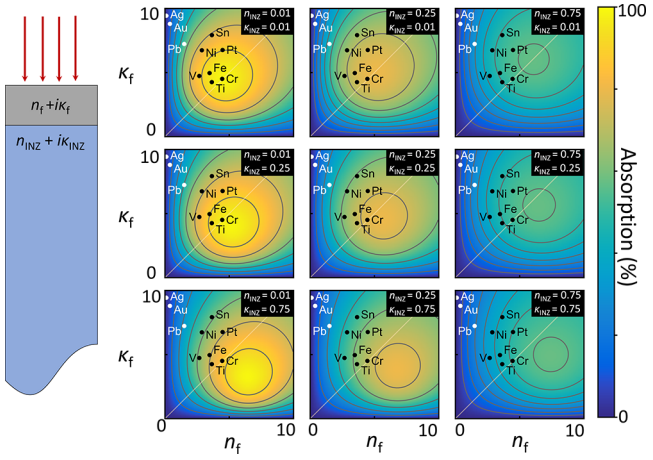

Figure 2. Effect of nonideal INZ on the absorption resonance. Numerically calculated absorption in a thin film ($n_f + i\kappa_f$) on an INZ substrate with $n_{INZ} + i\kappa_{INZ}$. The film is illuminated from air (see schematic). The diagonal line in each plot is the $n_f = \kappa_f$ line. Absorption is calculated for normal incidence at λ = 1300 nm for 5 nm thick films. Maximum absorption moves to higher n_f as κ_{INZ} increases, and the value of maximum absorption decreases with increasing n_{INZ}. The closed circles depict the optical indices of real materials, showing that the absorption peak moves away from common metals (toward higher n_f and lower κ_f) when there is high optical loss in the INZ material.

As n_{INZ} increases, the maximum absorption decreases. When illumination is incident from a high index material, such as silicon, the effects of n_{INZ} and κ_{INZ} on absorption are similar (see Supporting Information, Figure S1). Further, using the optical properties of real metals (Cr, Fe, Ti, and Pt) and INZ materials (ITO, AZO, and GZO) from literature,[6,9,18−20,33] we calculate that the thin film absorption can surpass ∼75% when illuminated through air and ∼90% when illuminated through silicon (see Figures S2 and S3).

Measured Absorption in Metal Films on INZ Substrates. We experimentally demonstrate the absorption enhancement in thin Pt films using a thick (>500 nm) AZO INZ substrate that was deposited using pulsed laser deposition both on glass and on a silicon substrate. A 2 cm × 2 cm silicon substrate was prepared with Al ohmic contacts and a 190 ± 5 nm Al_2O_3 antireflection coating on the top surface and Pt was deposited over the entire back surface. Part of the wafer was covered during the AZO deposition so the measurements with and without AZO were made on the same wafer, changing only the area of illumination (see Figure S4c for an image of the device).

To characterize the optical properties of AZO on the *n*-type Si/Pt wafer, we deposited AZO on a separate, bare Si substrate using identical deposition parameters. For absorption calculations, the AZO on Si was assumed to have the same properties as that deposited on the Si/Pt substrate. The thickness and refractive indices of the AZO were determined from ellipsometry fits using a general oscillator model, incorporating both Tauc-Lorentz and Drude models (Figure S3d,b). The AZO deposition created a thickness gradient, and the optical properties are dependent on the film thickness.[34] However, we found that the AZO thickness changes do not significantly impact the absorption within the Pt other than to shift the wavelength of maximum absorption because of the changes in the refractive indices of the AZO. Therefore, for the purposes of this work, we only consider the maximum thickness of the AZO on each device (note: the large area size and relative thickness uniformity of the maximum thickness regions allowed for easy laser alignment for absorption and responsivity measurements). After determining the optical properties of the AZO on glass, 5 ± 1 nm of Pt was deposited onto the AZO (note: for the Si substrates, 21 ± 2 nm of Pt was used to achieve the resonance condition).

The measured and calculated absorption of these devices shows a strong enhancement resulting from the INZ substrate (Figure 3). Note that the calculated absorption includes the

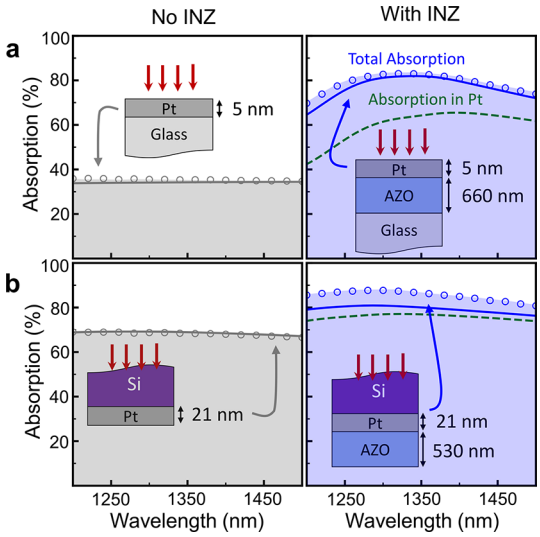

Figure 3. Measured and calculated absorption enhancement resulting from an index-near-zero substrate. Total absorption in thin film Pt without (left) and with (right) AZO when illuminated from (a) air and (b) silicon. The green dashed lines show absorption expected in only the Pt.

reflection loss from the antireflection coating on the top of the silicon surface. The experimental data (open circles) agree well with the calculated results for the total absorption in the devices both with AZO (blue solid lines) and without AZO (gray solid lines). The green dashed lines represent the calculated absorption within only the Pt for samples with AZO (note: both the glass and Si are transparent to NIR illumination). On average, AZO enhances the total absorption for the thin film Pt on glass by over a factor of 2 and by 26% for the Si/Pt photodiode.

For the sample illuminated from air, the calculations accurately determined the measurement results. However, the measured and calculated results for the *n*-Si/Pt photodiode have an absolute difference of ∼5% with higher measured absorption. This is likely due to slight differences in the AZO when deposited on Pt. Nevertheless, there is a clear enhancement in absorption within the Pt.

Enhanced Hot Electron Photodetection with an INZ Substrate. Photon absorption within the Pt film can lead to hot carrier generation and injection across the Si/Pt barrier, resulting in photocurrent. Near-IR radiation passes through the silicon wafer and is absorbed by the Pt contact (Figure 4a). The absorbed photons excite hot electrons, which travel to the interface and are injected into the silicon if it has energy larger than the Schottky barrier. The electrons then travel to the Al contact (which only covers a small region of the top surface) and are collected. Likewise, holes are collected through the Pt

DOI: 10.1021/acsphotonics.9b00449
ACS Photonics 2019, 6, 2238−2244

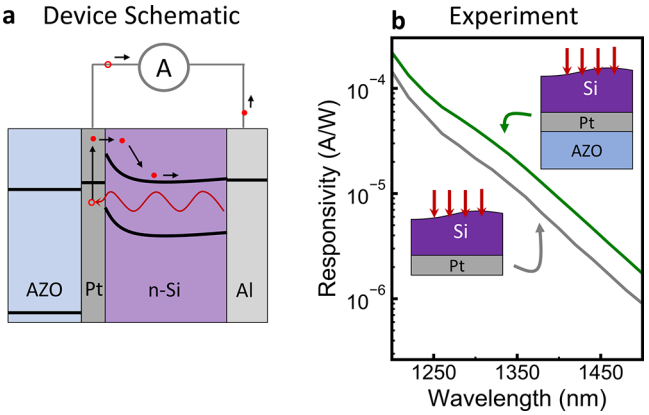

Figure 4. Enhanced hot carrier photocurrent with an index-near-zero substrate. (a) Schematic shows the photoresponse mechanism and band diagram for the Pt Schottky junction device. An absorbed photon excites a hot electron. The electron is injected into the silicon and collected through the ohmic Al contact. The hole is collected through the Pt contact. (b) Measured responsivity of the photodiode with (green) and without (gray) AZO. The photoresponse with the AZO is enhanced by >80%.

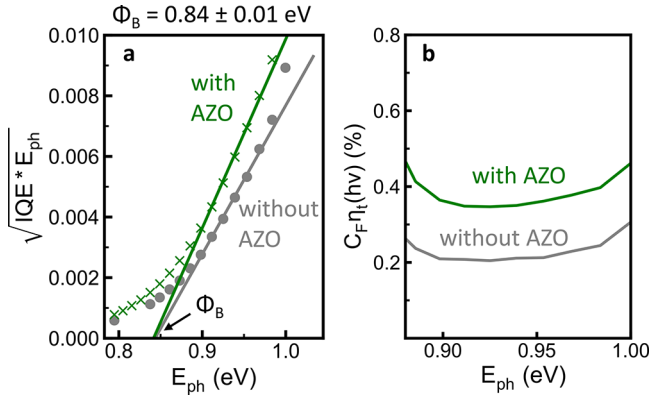

Figure 5. Barrier height and transport probability of the Si/Pt photodiode with and without AZO. (a) A barrier height of 0.84 ± 0.01 eV was determined from the linear fit to the Fowler yield (i.e., the square root of internal quantum efficiency). (b) The AZO contact nearly doubles the carrier transport probability.

contact. Because the diodes with and without AZO are on the same device, both measurements use the same contacts for consistency.

While the addition of an AZO layer to the back of the *n*-Si/Pt photodiode increases the absorption by 26%, the responsivity is enhanced by >80% (see Figure 4b), showing that the AZO layer is also affecting transport and carrier collection. The probability that a photoexcited electron will be collected is given by the internal quantum efficiency (IQE):

$$\mathrm{IQE}(h\nu) = A(h\nu)\eta_t(h\nu)\eta_F(h\nu) \tag{2}$$

where A is the absorption at photon energy $h\nu$, $\eta_t(h\nu)$ is the probability that the hot electron will reach the Schottky interface, and $\eta_F(h\nu)$ is the probability that the electron will have enough energy to traverse the barrier into the silicon substrate once it reached the interface. $\eta_F(h\nu)$ is known as the Fowler emission probability and is often calculated using a modified version of the Fowler yield equation:

$$\eta_F(h\nu) = C_F\frac{(h\nu - \Phi_B)^2}{h\nu} \tag{3}$$

where C_F is the Fowler coefficient and Φ_B is the Schottky barrier height. $\eta_t(h\nu)$ is dependent on factors such as electron mean free path, film thickness, and probability of multiple reflections from the film interfaces. C_F is a constant dependent on device geometry and Fermi energy. Therefore, the IQE is proportional to $(h\nu - \Phi_B)^2$ and can be used to determine the barrier height (Figure 5a), resulting in Φ_B = 0.84 ± 0.01 eV for both devices with and without the AZO.

A second method is also used to determine the barrier height from the forward current−voltage characteristic using thermionic emission theory, which results in a barrier height of 0.7 eV and an ideality factor of 3.56 (Figure S5).[35,36] This discrepancy between these two methods (and large ideality factor) along with the reduced barrier height from the expected 0.9 eV for a Pt/*n*-Si junction suggests that there is an interfacial region of PtSi and Pt_2Si reducing the quality of the junction and, hence, the responsivity.[36] However, the photodiodes with and without AZO will have the same interface because they were fabricated simultaneously on the same substrate. The consistency of the Schottky junctions is verified by their shared measured barrier height in Figure 5a.

We also extract $C_F \times \eta_t(h\nu)$ from the IQE characteristic and find that AZO enhances the probability that electrons will reach the Pt/*n*-Si Schottky interface by ∼70% on average (Figure 5b). Because the Pt film is very thin, the improved transport probability is likely due to a decrease in electron energy loss after reflection from the Pt/AZO interface. The carrier mean free path (MFP) in Pt is expected to be 10−20 nm;[37−40] therefore, our Pt film thickness is approximately equal to the MFP. Without the AZO, the carriers generated closer to the back of the Pt film are unlikely to reach the Si/Pt interface if they lose energy after scattering from absorbates or other contaminants at the Pt/air interface. However, with enhanced elastic scattering from the AZO Schottky barrier, carriers generated at the back of the film are more likely to reach the Si/Pt interface and traverse the barrier, effectively increasing the carrier transport probability.[41] We used heterodyne Kelvin probe force microscopy (KPFM) to determine the work function difference between the two materials,[42] and we find that AZO has 131 ± 75 mV larger work function than Pt (Figure S6). Additional work will be needed to determine the long-term stability of this effect, as the Pt will likely diffuse into the AZO over time.[43]

DISCUSSION

In summary, we have demonstrated that materials with refractive index-near-zero enhance the subwavelength FP-like resonance in ultrathin metallic films and can lead to increased hot carrier photocurrent. We experimentally verify a >2× absorption enhancement in Pt relative to a glass substrate and a 26% increase relative to a Si/Pt photodiode. We also found that the electrical response of the photodiode is enhanced by >80% due to a combination of increased absorption and improved carrier transport. To further enhance the responsivity of silicon-based, NIR hot carrier photodiodes, the diodes should be fabricated with significantly smaller surface area with consideration of edge effects by doping the silicon around the active area with a p-type dopant.[44] Reducing the temperature of the Pt and AZO deposition will also reduce the diffusion of the Pt into the silicon, improving the diode IV characteristics. Finding metals with similar optical properties to Pt, but with a

DOI: 10.1021/acsphotonics.9b00449
ACS Photonics 2019, 6, 2238−2244

longer mean free path would additionally enhance the photoresponse because of the increased probability of carrier collection after multiple reflections. Further, metals with appropriately chosen or tailored density of electron states can also improve hot carrier generation prior to transport and result in further photocurrent enhancements.[45]

Finally, this work further elucidates the physical mechanisms involved in enhancing the device response, which are important for optimal photodiode design. In addition to silicon-based diodes, the >2× enhancement in the Pt absorption on an AZO substrate illuminated from air suggests that it may be possible to design high efficiency metal−insulator−metal (MIM) near-IR detectors with Pt and AZO. The high absorption also requires significantly thinner Pt (4 nm as opposed to 17−20 nm) for the Si device. Therefore, an MIM device is likely to have higher emission probability after multiple hot carrier reflections because of the dual purposed (improved absorption and carrier transport) effects of the AZO layer.[46]

METHODS

Sample Fabrication. The platinum/*n*-type silicon photodiode was fabricated on a 370 μm thick, double-side polished, ⟨100⟩ *n*-type silicon wafer (<1 Ω·cm). Wafers were cleaned in a piranha etch (3:1 sulfuric acid (H_2SO_4) and hydrogen peroxide (H_2O_2)) to remove all organic material, a buffered oxide etch (BOE) to remove the native oxide, and dried under a N_2 stream. Immediately after the cleaning procedure, ohmic contacts were formed by depositing aluminum (Al) through a shadow mask in a thin strip along the top surface of each device, which was annealed at 425 °C in a forming gas of 96% Ar and 4% H_2. A ∼190 nm Al_2O_3 antireflection coating was then deposited using atomic layer deposition, keeping the Al uncoated to enable electrical connection to the device. The native oxide was removed from the back surface of the Si with BOE, and 21 nm of Pt was deposited using an Angstrom e-beam evaporator at a deposition rate of ∼1.4 Å s^{-1} at a base pressure of ∼2 × 10^{-6} Torr. Finally, 530 nm of AZO was deposited over 80% of the Pt area using pulsed laser deposition. The 2 wt % AZO target were purchased from the Kurt J. Lesker Corp. with purities of 99.99% or higher. The energy density of the laser beam at the target surface was maintained at 1.0 J/cm^2 and the substrate temperature was 400 °C.

For illumination from air, 660 nm of AZO was deposited on a standard glass microscope slide using pulsed laser deposition. After optical characterization, 5 nm of Pt was deposited over the top of the AZO using an Angstrom e-beam evaporator at a deposition rate of ∼1 Å s^{-1} at a base pressure of ∼3.7 × 10^{-6} Torr.

Material Characterization. During each Pt deposition, a microscope slide was included in the deposition to determine the thickness and refractive index of the deposited metal. All material refractive indices and thicknesses were determined using a J. A. Woollam M-2000D Spectroscopic Ellipsometer, 8″ (190−1700 nm).

Optical and Electrical Measurements. Absorption measurements were performed using a 6 in. integrating sphere (Labsphere RTC-060) with illumination at near-normal incidence of 12°. Two Ge photodiodes were used to measure the light intensity inside the integrating sphere and to monitor power fluctuations of the incident beam. Specific NIR wavelengths were selected from a supercontinuum source (Fianium WhiteLase) using an acousto-optic tunable filter (AOTF), and the incident light was chopped using a rotating disk chopper. The signals from the photodiodes were measured using a SR830 lock-in amplifier with the reference frequency matched to the frequency of the optical chopper. The uncertainty of the measured absorption is ±0.5%. To determine the responsivity of the fabricated photodiode, the sample was mounted on a vertical stage with copper probes forming electrical contact to the Al ohmic and Pt contacts. The incident light was focused on the sample at normal incidence and the power incident on the sample was determined by a calibrated InGaAs photodiode. The incident power was on the order of 1 μW for all wavelengths. The signals from the sample and each photodiode were measured using a SR830 lock-in amplifier with the reference frequency matched to the frequency of the optical chopper. There is a 2−3% uncertainty in the measured responsivity.

Optical Calculations. The theoretical absorption was calculated for near-normal incidence, that is, ∼12°, using the transfer matrix method assuming that the glass and silicon substrates are infinite. To account for the incident reflection from the air/Al_2O_3/silicon interface, the calculated total absorption for the Si/Pt device was corrected to accurately describe the measured absorption using $A_T^{cor} = A_T - R_{ARC}$, where A_T^{cor} is the corrected total absorption, A_T is the total uncorrected absorption of the device assuming illumination through infinitely thick silicon, and R_{ARC} is the reflection from the Al_2O_3 antireflection coating (ARC). R_{ARC} is determined from optical properties of Al_2O_3 measured using ellipsometry. The calculated absorption within the Pt when there is an AZO back contact (green dotted line in Figure 3B) is also corrected for the initial reflection loss using the following equation: $A_{Pt}^{cor} = \frac{A_{Pt}}{A_T} \times A_T^{cor}$, where A_{Pt}^{cor} is the absorption in the thin film Pt corrected for reflection from the ARC coating and A_{Pt} is the uncorrected absorption in Pt calculated with the assumption that it is illuminated through infinitely thick silicon.

KPFM Measurements. The heterodyne Kelvin probe force microscopy measurements were performed using a Cypher atomic force microscope with a CSC37/Pt probe. An AC voltage of 3 V was applied to generate a potential difference between the probe and the sample's surface at a frequency of 226.97 kHz. The frequencies at which the H-KPFM signal was detected and the probe was oscillated to control the topography are 195.9 kHz and 31.075 kHz, respectively.

ASSOCIATED CONTENT

Supporting Information

The Supporting Information is available free of charge on the ACS Publications website at DOI: 10.1021/acsphotonics.9b00449.

Explanation of the transfer matrix method. Effect of nonideal INZ on the absorption resonance when $n_{top} = n_{Si}$. Optical design considerations for INZ materials to enhance absorption in Pt and Cr. Absorption in Pt, Ti, Cr, and Fe on INZ substrates with optical properties found in literature. AZO has index-near-zero behavior. Current−voltage relationship for the Si/Pt photodiode. Kelvin probe force microscopy scan of Pt and AZO edge (PDF)

DOI: 10.1021/acsphotonics.9b00449
ACS Photonics 2019, 6, 2238−2244

AUTHOR INFORMATION

Corresponding Author

*E-mail: jnmunday@umd.edu.

ORCID

Lisa J. Krayer: 0000-0001-9133-226X
Jongbum Kim: 0000-0002-5914-8910
Joseph L. Garrett: 0000-0001-8265-0661
Jeremy N. Munday: 0000-0002-0881-9876

Author Contributions

J.N.M. conceived and managed the project. J.K. fabricated the AZO films. J.L.G. performed AFM measurements. L.J.K. performed all mathematical analysis and completed all other fabrication, measurements, and analysis. All authors discussed and commented on the manuscript.

Funding

This material is based on work supported by the National Science Foundation CAREER Grant No. ECCS-1554503 and the Office of Naval Research YIP Award under Grant No. N00014-16-1-2540. L.J.K. is supported by an NSF Graduate Research Fellowship (DGE 1322106, ECCS-1554503) and an Ann G. Wylie Dissertation Fellowship.

Notes

The authors declare no competing financial interest.

ACKNOWLEDGMENTS

We thank the FabLab at the Maryland Nanocenter for access to all fabrication equipment including, but not limited to, the e-beam evaporator and Woollam Spectroscopic Ellipsometer. We thank Professor Ichiro Takeuchi for sharing the pulsed laser deposition system.

REFERENCES

(1) Liberal, I.; Engheta, N. Near-Zero Refractive Index Photonics. *Nat. Photonics* **2017**, *11*, 149−158.
(2) Edwards, B.; Alù, A.; Young, M. E.; Silveirinha, M.; Engheta, N. Experimental Verification of Epsilon-Near-Zero Metamaterial Coupling and Energy Squeezing Using a Microwave Waveguide. *Phys. Rev. Lett.* **2008**, *100*, 033903.
(3) Adams, D. C.; Inampudi, S.; Ribaudo, T.; Slocum, D.; Vangala, S.; Kuhta, N. A.; Goodhue, W. D.; Podolskiy, V. A.; Wasserman, D. Funneling Light through a Subwavelength Aperture with Epsilon-near-Zero Materials. *Phys. Rev. Lett.* **2011**, *107*, 1−5.
(4) Halterman, K.; Feng, S. Resonant Transmission of Electromagnetic Fields through Subwavelength Zero- Slits. *Phys. Rev. A: At., Mol., Opt. Phys.* **2008**, *78*, 1−4.
(5) Nguyen, V. C.; Chen, L.; Halterman, K. Total Transmission and Total Reflection by Zero Index Metamaterials with Defects. *Phys. Rev. Lett.* **2010**, *105*, 1−4.
(6) Capretti, A.; Wang, Y.; Engheta, N.; Dal Negro, L. Enhanced Third-Harmonic Generation in Si-Compatible Epsilon-near-Zero Indium Tin Oxide Nanolayers. *Opt. Lett.* **2015**, *40*, 1500.
(7) Argyropoulos, C.; Chen, P.-Y.; D'Aguanno, G.; Engheta, N.; Alù, A. Boosting Optical Nonlinearities in ϵ-near-Zero Plasmonic Channels. *Phys. Rev. B: Condens. Matter Mater. Phys.* **2012**, *85*, 045129.
(8) Traviss, D.; Bruck, R.; Mills, B.; Abb, M.; Muskens, O. L. Ultrafast Plasmonics Using Transparent Conductive Oxide Hybrids in the Epsilon-near-Zero Regime. *Appl. Phys. Lett.* **2013**, *102*, 121112.
(9) Kim, J.; Dutta, A.; Naik, G. V.; Giles, A. J.; Bezares, F. J.; Ellis, C. T.; Tischler, J. G.; Mahmoud, A. M.; Caglayan, H.; Glembocki, O. J.; et al. Role of Epsilon-near-Zero Substrates in the Optical Response of Plasmonic Antennas. *Optica* **2016**, *3*, 339.
(10) Feng, S.; Halterman, K. Coherent Perfect Absorption in Epsilon-near-Zero Metamaterials. *Phys. Rev. B: Condens. Matter Mater. Phys.* **2012**, *86*, 165103.
(11) Vassant, S.; Archambault, A.; Marquier, F.; Pardo, F.; Gennser, U.; Cavanna, A.; Pelouard, J. L.; Greffet, J. J. Epsilon-Near-Zero Mode for Active Optoelectronic Devices. *Phys. Rev. Lett.* **2012**, *109*, 237401.
(12) Vasudev, A. P.; Kang, J.-H.; Park, J.; Liu, X.; Brongersma, M. L. Electro-Optical Modulation of a Silicon Waveguide with an "Epsilon-near-Zero" Material. *Opt. Express* **2013**, *21*, 26387.
(13) Zhao, H.; Wang, Y.; Capretti, A.; Negro, L. D.; Klamkin, J. Broadband Electroabsorption Modulators Design Based on Epsilon-Near-Zero Indium Tin Oxide. *IEEE J. Sel. Top. Quantum Electron.* **2015**, *21*, 192−198.
(14) Jun, Y. C.; Reno, J.; Ribaudo, T.; Shaner, E.; Greffet, J.-J.; Vassant, S.; Marquier, F.; Sinclair, M.; Brener, I. Epsilon-Near-Zero Strong Coupling in Metamaterial-Semiconductor Hybrid Structures. *Nano Lett.* **2013**, *13*, 5391−5396.
(15) Krayer, L. J.; Tennyson, E. M.; Leite, M. S.; Munday, J. N. Near-IR Imaging Based on Hot Carrier Generation in Nanometer-Scale Optical Coatings. *ACS Photonics* **2018**, *5*, 306−311.
(16) Güsken, N. A.; Lauri, A.; Li, Y.; Matsui, T.; Doiron, B.; Bower, R.; Regoutz, A.; Mihai, A.; Petrov, P. K.; Oulton, R. F.; et al. TiO_{2-x}-Enhanced IR Hot Carrier Based Photodetection in Metal Thin Film−Si Junctions. *ACS Photonics* **2019**, *6*, 953−960.
(17) Rensberg, J.; Zhou, Y.; Richter, S.; Wan, C.; Zhang, S.; Schöppe, P.; Schmidt-Grund, R.; Ramanathan, S.; Capasso, F.; Kats, M. A.; et al. Epsilon-Near-Zero Substrate Engineering for Ultrathin-Film Perfect Absorbers. *Phys. Rev. Appl.* **2017**, *8*, 014009.
(18) Kim, J.; Naik, G. V.; Gavrilenko, A. V.; Dondapati, K.; Gavrilenko, V. I.; Prokes, S. M.; Glembocki, O. J.; Shalaev, V. M.; Boltasseva, A. Optical Properties of Gallium-Doped Zinc Oxide—A Low-Loss Plasmonic Material: First-Principles Theory and Experiment. *Phys. Rev. X* **2013**, *3*, 041037.
(19) Alam, M. Z.; De Leon, I.; Boyd, R. W. Large Optical Nonlinearity of Indium Tin Oxide in Its Epsilon-near-Zero Region. *Science* **2016**, *352*, 795−797.
(20) Chen, C.; Wang, Z.; Wu, K.; Ye, H. Tunable Near-Infrared Epsilon-near-Zero and Plasmonic Properties of Ag-ITO Co-Sputtered Composite Films. *Sci. Technol. Adv. Mater.* **2018**, *19*, 174−184.
(21) Krayer, L. J.; Kim, J.; Munday, J. N. Near-Perfect Absorption throughout the Visible Using Ultra-Thin Metal Films on Index-near-Zero Substrates [Invited]. *Opt. Mater. Express* **2019**, *9*, 330.
(22) Hägglund, C.; Apell, S. P.; Kasemo, B. Maximized Optical Absorption in Ultrathin Films and Its Application to Plasmon-Based Two-Dimensional Photovoltaics. *Nano Lett.* **2010**, *10*, 3135−3141.
(23) Kats, M. A.; Blanchard, R.; Genevet, P.; Capasso, F. Nanometre Optical Coatings Based on Strong Interference Effects in Highly Absorbing Media. *Nat. Mater.* **2013**, *12*, 20−24.
(24) Kats, M. A.; Blanchard, R.; Ramanathan, S.; Capasso, F. Thin-Film Interference in Lossy, Ultra-Thin Layers. *Opt. Photonics News* **2014**, *25*, 40.
(25) Mirshafieyan, S. S.; Guo, J. Silicon Colors: Spectral Selective Perfect Light Absorption in Single Layer Silicon Films on Aluminum Surface and Its Thermal Tunability. *Opt. Express* **2014**, *22*, 31545.
(26) Dias, M. R. S.; Gong, C.; Benson, Z. A.; Leite, M. S. Lithography-Free, Omnidirectional, CMOS-Compatible AlCu Alloys for Thin-Film Superabsorbers. *Adv. Opt. Mater.* **2018**, *6*, 1700830.
(27) Ahmad, N.; Stokes, J.; Fox, N. A.; Teng, M.; Cryan, M. J. Ultra-Thin Metal Films for Enhanced Solar Absorption. *Nano Energy* **2012**, *1*, 777−782.
(28) Krayer, L. J.; Tennyson, E. M.; Leite, M. S.; Munday, J. N. Near-IR Imaging Based on Hot Carrier Generation in Nanometer-Scale Optical Coatings. *ACS Photonics* **2018**, *5*, 306−311.
(29) Born, M.; Wolf, E. *Principles of Optics*, 7th ed.; Cambridge University Press, 1999.
(30) Johnson, P. B.; Christy, R. W. Optical Constants of the Noble Metals. *Phys. Rev. B* **1972**, *6*, 4370−4379.
(31) Palik, E. D. *Handbook of Optical Constants of Solids, I-III*; Elsevier, Inc.: Amsterdam, 1998.

DOI: 10.1021/acsphotonics.9b00449
ACS Photonics 2019, 6, 2238−2244

(32) Weaver, J. H.; Colavita, E.; Lynch, D. W.; Rosei, R. Low-Energy Interband Absorption in Bcc Fe and Hcp Co. *Phys. Rev. B: Condens. Matter Mater. Phys.* **1979**, *19*, 3850−3856.
(33) Kim, J.; Naik, G. V.; Emani, N. K.; Guler, U.; Boltasseva, A. Plasmonic Resonances in Nanostructured Transparent Conducting Oxide Films. *IEEE J. Sel. Top. Quantum Electron.* **2013**, *19*, 4601907−4601907.
(34) Naik, G. V.; Kim, J.; Boltasseva, A. Oxides and Nitrides as Alternative Plasmonic Materials in the Optical Range [Invited]. *Opt. Mater. Express* **2011**, *1*, 1090.
(35) Cheung, S. K.; Cheung, N. W. Extraction of Schottky Diode Parameters from Forward Current-voltage Characteristics. *Appl. Phys. Lett.* **1986**, *49*, 85−87.
(36) Sze, S. M.; Ng, K. K. *Physics of Semiconductor Devices*: 3rd ed.; Wiley, 2007.
(37) Vlutters, R.; van 't Erve, O. M. J.; Jansen, R.; Kim, S. D.; Lodder, J. C.; Vedyayev, A.; Dieny, B. Modeling of Spin-Dependent Hot-Electron Transport in the Spin-Valve Transistor. *Phys. Rev. B: Condens. Matter Mater. Phys.* **2001**, *65*, 024416.
(38) Niedermann, P.; Quattropani, L.; Solt, K.; Maggio-Aprile, I.; Fischer, O. Hot-Carrier Scattering in a Metal: A Ballistic-Electron-Emission Microscopy Investigation on PtSi. *Phys. Rev. B: Condens. Matter Mater. Phys.* **1993**, *48*, 8833−8839.
(39) Zhukov, V. P.; Chulkov, E. V.; Echenique, P. M. Lifetimes and Inelastic Mean Free Path of Low-Energy Excited Electrons in Fe, Ni, Pt, and Au: Ab Initio GW+ T Calculations. *Phys. Rev. B: Condens. Matter Mater. Phys.* **2006**, *73*, 125105.
(40) Fischer, G.; Hoffmann, H.; Vancea, J. Mean Free Path and Density of Conductance Electrons in Platinum Determined by the Size Effect in Extremely Thin Films. *Phys. Rev. B: Condens. Matter Mater. Phys.* **1980**, *22*, 6065−6074.
(41) Scales, C.; Berini, P. Thin-Film Schottky Barrier Photodetector Models. *IEEE J. Quantum Electron.* **2010**, *46*, 633−643.
(42) Garrett, J. L.; Munday, J. N. Fast, High-Resolution Surface Potential Measurements in Air with Heterodyne Kelvin Probe Force Microscopy. *Nanotechnology* **2016**, *27*, 245705.
(43) Schultz, T.; Vogt, S.; Schlupp, P.; von Wenckstern, H.; Koch, N.; Grundmann, M. Influence of Oxygen Deficiency on the Rectifying Behavior of Transparent-Semiconducting-Oxide−Metal Interfaces. *Phys. Rev. Appl.* **2018**, *9*, 064001.
(44) Tove, P. A.; Hyder, S. A.; Susila, G. Diode Characteristics and Edge Effects of Metal-Semiconductor Diodes. *Solid-State Electron.* **1973**, *16*, 513−521.
(45) Gong, T.; Munday, J. N. Materials for Hot Carrier Plasmonics [Invited]. *Opt. Mater. Express* **2015**, *5*, 2501.
(46) Gong, T.; Munday, J. N. Angle-Independent Hot Carrier Generation and Collection Using Transparent Conducting Oxides. *Nano Lett.* **2015**, *15*, 147−152.

DOI: 10.1021/acsphotonics.9b00449
ACS Photonics 2019, 6, 2238−2244